WARSAW UNIVERSITY OF TECHNOLOGY Index 351733
FACULTY OF CIVIL ENGINEERING
COMMITTEE FOR CIVIL AND WATER ENGINEERING
POLISH ACADEMY OF SCIENCES ISSN 1230-2945

DOI: 10.24425/ace.2022.140191

ARCHIVES OF CIVIL ENGINEERING

Vol. LXVIII ISSUE 1 2022

pp. 635 –651

Research paper

Study on stress characteristics of deep roadway bolt based on nonlinear dilatancy angle model

Zenghua Lin[1]

Abstract: Full-length bonded bolts are widely used in deep mining engineering and an in-depth understanding of their mechanical characteristics under complex and high ground stress conditions is of great significance for deep roadway support systems. Based on a quantitative GSI rating system of surrounding rocks and rock nonlinear dilatancy angle model, a nonlinear dilatancy angle model suitable for jointed rocks was developed. The Hoek–Brown strain-softening model parameters were transformed into equivalent Mohr–Coulomb strength parameters, and a numerical model of the deep roadway was constructed using FLAC^{3D} numerical simulation software as a tool. The force characteristics of full-length bonded anchors under different constitutive model and dilatancy angle model conditions were analyzed, and the effects of different lengths of anchors on the stability of the surrounding rock were studied. The obtained results revealed a big difference between the axial forces of bolts calculated by strain-softening and ideal elastic-plastic models. It was also found that bolt shear force was less influenced by the strain-softening behaviors of surrounding rocks. Dilatancy angle greatly affected bolt axial force. Therefore, if the dilatancy angle was neglected, great errors would be created in the calculation results of supporting structure designs. The nonlinear dilatancy angle model of jointed rock masses more accurately captured the stress properties of bolts after field monitoring and analysis. The findings of the study can serve as a guide for calculating the stability of surrounding rocks in deep mining engineering.

Keywords: deep roadway, full-length bond bolt, strain-softening, nonlinear dilating angle, numerical simulation

[1]Lec., MSc., Eng., School of Civil Engineering, University of Science and Technology Liaoning, China, e-mail: linzenghua520@163.comc ORCID: 0000-0003-2542-4902

1. Introduction

In coal mining, especially in designing and constructing support systems for surrounding rocks of deep roadways, bolts are the main support structures. Under the action of anchor bolts, the stress state and strength parameters of surrounding rocks can change and bolts play critical roles in the reinforcement of surrounding rocks [1, 2]. In practical roadway support engineering, end-anchored bolts are the most widely used bolt type. For full-length bonded bolts, due to their complex structures and high construction costs, it takes a long time for the mortar to reach standard strength after grouting. Therefore, their application in shallow excavation engineering is limited. In deep soft rock roadway support systems, end-anchored bolts cannot control large deformations of surrounding rocks [3]. Under such conditions, however, full-length bonded bots play a key role in controlling surrounding rock stability. Despite their importance, relatively few studies have been performed on their mechanical characteristics in deep soft rocks, especially considering deep rock masses under the condition of strain softening and dilatancy.

Researchers have mainly focused on the mechanical characteristics of full-length bond bolts in experimental research and theoretical analyses and have obtained a large number of data. In experimental studies, Shi et al. proposed a non-destructive acoustic testing signal analysis method for bond bolts based on Hilbert–Huang transformation (HHT), which was capable of identifying grouting defect location and bolt length using noise signals of multiple reflection interfaces [4]. Feng et al. conducted bolt drawing tests under different pre-tightening forces and found that pre-tightening all-bond bolts were more durable and stable than end-sealing resin bolts in supporting systems adopted in most coal mines [5]. Yang et al. analyzed the shear stress of bolts during shear displacement based on the deformation and failure properties of jointed rock masses [6]. Wu et al. performed a series of bolt dynamic response tests based on the SHPB system and studied the mechanical response characteristics of full-length binding bolts under dynamic disturbance [7].

In terms of theoretical analysis, Liu et al. used a 3D linear model and local deformation theory, the change process of the full-length bond anchorage interface was divided into elastic, plastic softening and crack slip stages [8]. Oreste improved the existing full-length bond bolt model by introducing the Hoek–Brown strength criterion and applied it to a wider range of rock types [9]. Yao et al. used surrounding rock displacements in tunnels as a parameter and obtained the shear stress of the anchor interface due to surrounding rock deformations. Neutral point axial forces were used as concentrated force sources, and shear stress distribution at the anchor interface was obtained from Mindlin solution of a semi-infinite body under concentrated force [10]. Zhao et al. analyzed the force characteristics of full-length bonded anchors using a nonlinear dilatancy angle model and verified the reliability of this model through on-site monitoring [11].

The above research provided a theoretical basis for understanding the interaction between full-length bonded anchors and rock masses, but the mechanical properties and stress conditions of deep surrounding rocks were simplified in calculations. In deep mining, anchors often fail due to high ground stresses. Therefore, in order to better optimize

the support design of surrounding rocks in roadways, it is necessary to determine the force characteristics of full-length bonded anchors under high ground stress.

Salehnia et al. investigated dilatancy angle and proposed a new equation which related dilatancy angle to plastic shear strain during loading [12]. Cheng et al. derived the direct equation describing the relationship of expansion angle and surrounding rock deformation based on the latest theoretical research results [13]. Zhao et al. derived the relationship between expansion angle and confining pressure through expansion index and established an expansion model for heterogeneous rocks with confining stress [14]. Wang et al. used plastic theory and nonlinear fitting method to develop a two-parameter expansion angle model based on the effect of confining pressure and plasticity parameters using three-axis loading and unloading cycle test data obtained from Jinping marble [15]. Alejano proposed a dilatancy angle model by performing a comprehensive analysis on experimental data. The proposed model reflected the strain behavior of rock specimens in compression tests and could be used to solve tunnel foundation reaction curves in poor to medium-mass rocks [16, 17].

Based on previous studies using the Quantifying GSI Surrounding Rock Rating System and rock nonlinear dilatancy model, this paper proposed a nonlinear dilatancy angle model suitable for jointed rock masses and converted Hoek–Brown strain-softening model parameters into equivalent Mohr–Coulomb strength parameters. A numerical model for surrounding rocks in deep roadways was constructed using FLAC^{3D} numerical simulation software as a tool to analyze the mechanical characteristics of full-length bonded anchors under different constitutive and dilatancy angle models. It also provided a reference for the analysis and calculation of surrounding rock stability in deep engineering.

2. Nonlinear dilatancy angle model of rock masses based on quantitative GSI system

2.1. Quantifying GSI surrounding rock rating system

Proper determination of the mechanical parameters of rock masses plays a critical role in the reliability of underground engineering designs. Among various surrounding rock rating methods, the RMR (Relative Metabolic Rate) method is very suitable for engineering quality evaluation of jointed rock masses and is convenient for obtaining the quality grade of jointed rock masses. However, Hoek and Brown found that RMR value could not give a reasonable evaluation value for weak and broken rock mass structures with poor qualities in a large number of engineering practices. Therefore, Hoek and Brown replaced the RMR system with GSI surrounding rock rating system [18]. With the extensive use and continuous improvement of GSI surrounding rock rating system, a quantitative GSI surrounding rock classification method was proposed by Cai et al. based on block size V_b and structural surface condition factor J_c, which made the determination of GSI values more objective, as shown in Fig. 1 [19].

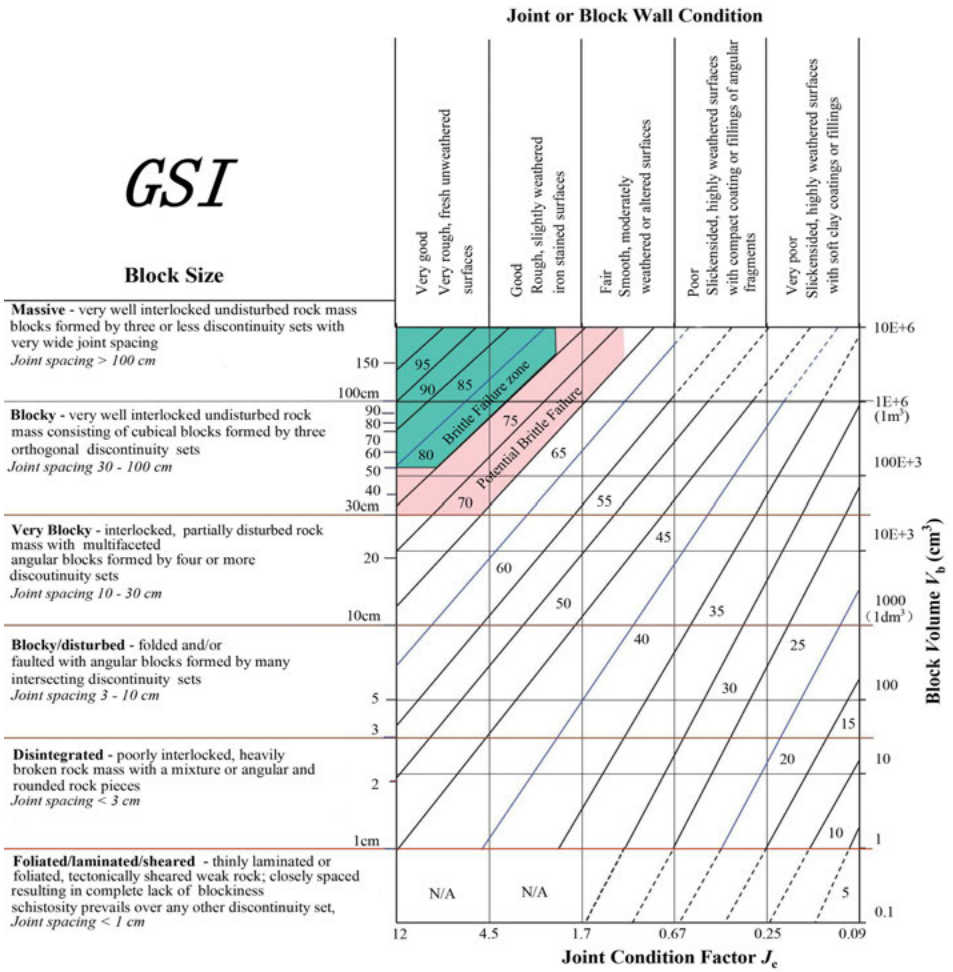

Fig. 1. Schematic diagram of quantifying GSI surrounding rock rating system

The quantized GSI system consists of multiple condition factors, which are separately solved by establishing corresponding relations. Among them, the size and volume of rock blocks are calculated according to the combination of direction, spacing, and a number of joints, which are important indices for evaluating rock mass quality [20].

2.2. Post-peak mechanical characteristics of rock masses based on GSI system

Strength parameters of rock masses gradually change during the yield failure process. The intensity decay process is difficult to express in theory. Many engineering calculations are based on classical elastoplastic theory or idealized strain-softening model. Hoek et

al. found in engineering practice that the post-peak behavior of jointed rock masses was related to geological strength index GSI [18]. As shown in Fig. 2, during the unloading process, when GSI > 75, rock mass exhibited elastic brittle behavior while when 25 < GSI < 75, it exhibited strain-softening behavior, and when GSI < 25, rock mass showed ideal elastoplastic behavior, and it was considered that the dilatancy angle of the rock mass was zero at this time and the expansion and strain-softening behavior of jointed rock masses were disappeared.

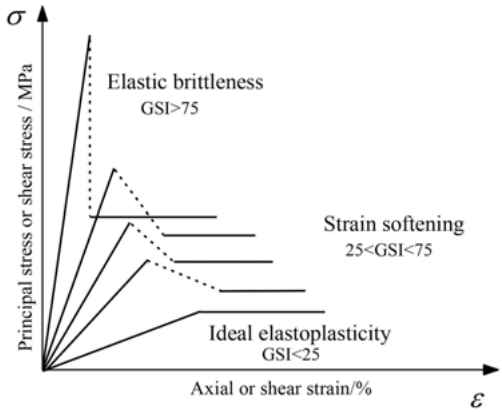

Fig. 2. Post-peak mechanical model of jointed rock masses based on GSI

In the process of yield damage, whether the rock is intact or moderately or highly jointed, the damage will produce a plastic shear fracture zone, thus transforming the rock from more intact to more or extremely fractured. It can also be expressed by the GSI system and converted into Hoek–Brown model parameters. Rock mass V_b and structural surface condition factor J_c are degenerate during the softening and damage processes and jointed rock mass GSI indices are linearly decreased from the peak GSI^p conversion to post-peak residual GSI^r. Fig. 3 shows a schematic diagram of the degradation process of the GSI index of jointed rock masses.

Cai et al. performed a large number of indoor triaxial tests and large-scale underground structure engineering to analyze post-peak residuals $\mathrm{GSI}^{\mathrm{res}}$ and proposed the available peak values of rock $\mathrm{GSI}^{\mathrm{peak}}$ and post-peak residuals $\mathrm{GSI}^{\mathrm{res}}$ range [21]. When peak rock size was $V_b > 10\ \mathrm{cm}^3$, the average rock mass size in the plastic residual stage was considered to be $V_b^r = 10\ \mathrm{cm}^3$. When peak rock mass size is $V_b \leq 10\ \mathrm{cm}^3$, the average rock mass size in the plastic residual stage can be assumed to remain unchanged; that is, $V_b^r = V_b$. Rock surface condition factor J_c is also decreased during the failure process. Cai et al. then developed a quantitative method for the calculation of the residual GSI^r indices of rock masses which can be used in actual engineering applications and verified by large-scale in-situ tests. Based on this, Alejano fitted the empirical relationship between peak GSI^p and residual GSI^r as [22]:

$$\mathrm{GSI}^r = 17.25 \cdot \mathrm{e}^{0.0107 \cdot \mathrm{GSI}^p} \tag{2.1}$$

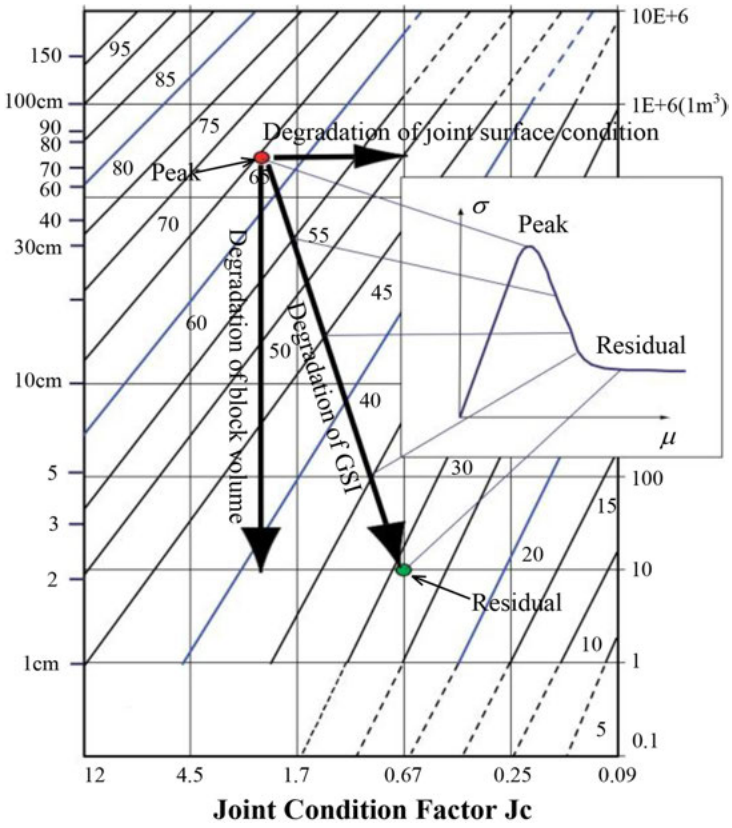

Fig. 3. Schematic diagram of the degradation process of GSI indicators

2.3. Nonlinear dilatancy angle model of rock mass based on GSI system

2.3.1. Unloading process of surrounding rock in cavern

As can be seen in Fig. 4a, a strain-softening zone and a residual strength zone were formed after the excavation unloading of roadway surrounding rock. During excavation and unloading processes, surrounding rock was transformed from the stress state of the original rock (point A) to the peak GSI^p of the elastic stage (pointB), and after joint fissure expansion and softening (point C), it was transformed into the residual GSI^r of plastic residual phase (point D). According to the gradual evolution of surrounding rock strength parameters, plastic shear strain γ^p was closely related to σ_3 and σ_3 was determined by virtual support pressure p_i obtained from working face and support pressure p_i^{**} of the support system. As shown in Fig. 4b, in the H-B principal stress curve, when support pressure p_i decreased to p_i^*, the surrounding rock entered the plastic softening stage and thereafter p_i changed in the range of p_i^*–p_i^{**}.

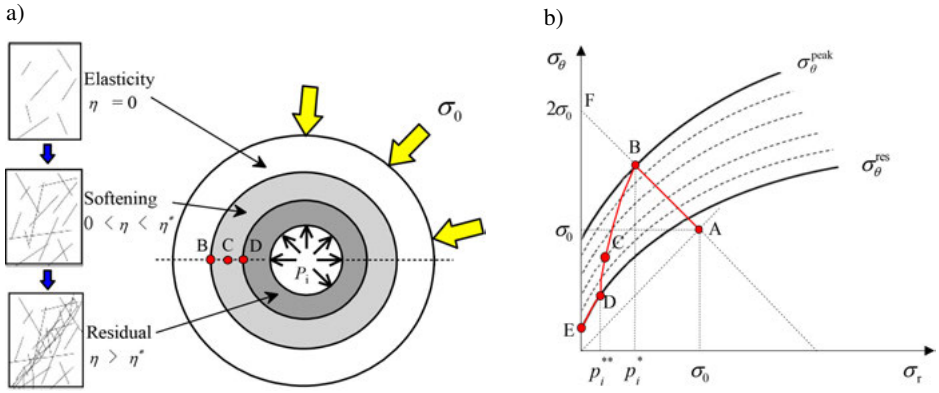

Fig. 4. Rock mass softening and residual areas: a) softening and residual areas of surrounding rock in cavern, b) Hoek–Brown principal stress curve

2.3.2. Dilatancy angle model considering strain-softening of rock mass

Mohr–Coulomb yield criterion can be expressed as:

$$f(\sigma_\theta, \sigma_r, \eta) = \sigma_\theta - K_\varphi(\eta)\sigma_r - \sigma_c \tag{2.2}$$

where σ_c is rock uniaxial compressive strength, such that:

$$\sigma_c = 2c(\eta)\sqrt{K_\varphi(\eta)} \tag{2.3}$$

$$K_\varphi = \frac{1+\sin\varphi}{1-\sin\varphi} \tag{2.4}$$

Hoek–Brown and Mohr–Coulomb strain-softening relationships can be expressed as:

$$\omega(\eta) = \begin{cases} \omega^p - \dfrac{\omega^p - \omega^r}{\eta^*}\eta & 0 < \eta < \eta^* \\ \omega^r, & \eta \geq \eta^* \end{cases}. \tag{2.5}$$

where ω^p is peak parameter, ω^r is a residual parameter, and η^* is the critical softening parameter value of the rock transitioning from strain-softening to residual phase. ω can replace cohesion force c and friction angle φ, and can also replace m_b.

As can be seen from Fig. 5, when $\eta = 0$, rock mass and contact surface were in the elastic deformation stage, $0 < \eta < \eta^*$ represented strain-softening stage, and $\eta > \eta^*$ implied residual stage; the softening process of rock was controlled by slope M which is the softening modulus of rock.

Plasticity parameter η^* was derived based on the difference between the maximum and minimum principal plastic strains, that is:

$$\gamma^p = \eta^* = \varepsilon_1^p - \varepsilon_3^p \tag{2.6}$$

where γ^p is plastic shear strain, and ε_1^p and ε_3^p are maximum and minimum values of plastic strain, respectively.

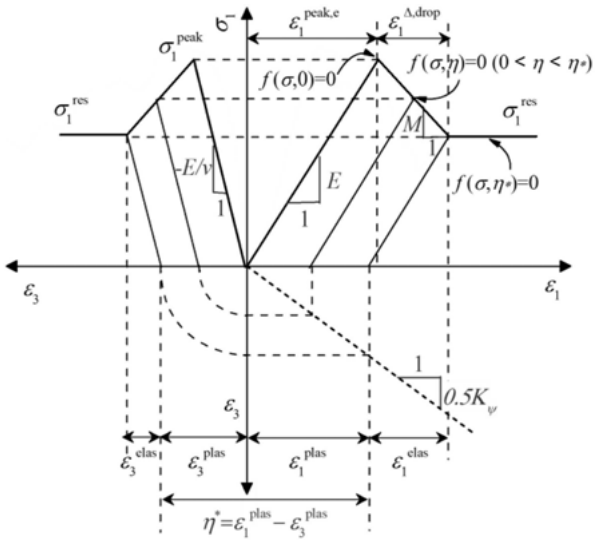

Fig. 5. Strain-softening curves of rock

According to the simplified strain-softening curve after rock peak in Fig. 5, the maximum principal plastic strain ε_1^p can be expressed as:

$$\varepsilon_1^p = \varepsilon_1^{\text{peak},e} + \varepsilon_1^{\Delta,\text{drop}} - \varepsilon_1^e \tag{2.7}$$

where $\varepsilon_1^{\text{peak},e}$ is the pre-peak elastic maximum principal strain, $\varepsilon_1^{\text{drop}}$ is the post-peak softening strain, and ε_1^e is the elastic maximum principal strain. When confining pressure σ_3 is constant, the parameters in Eq. (2.7) can be expressed as:

$$\begin{cases} \varepsilon_1^{\text{peak},e} = \dfrac{\sigma_1^p(\sigma_3)}{E} \\ \varepsilon_1^{\text{drop}} = \dfrac{\sigma_1^p(\sigma_3) - \sigma_1^r(\sigma_3)}{-M} \\ \varepsilon_1^e = \dfrac{\sigma_1^r(\sigma_3)}{E} \end{cases} \tag{2.8}$$

where σ_1^p and σ_1^r are peak and residual principal stress, respectively.

In numerical calculations, softening modulus M of rock and structural surfaces can be obtained by fitting the stress-strain curves of rock samples of each rock stratum obtained from the test.

Considering the volumetric deformation of rock mass, it is necessary to introduce dilatancy angle ψ. Alonso et al. proposed an expansion angle equation based on the Hoek's study as [23]:

$$\psi = \frac{5\text{GSI} - 125}{1000}\varphi \tag{2.9}$$

where φ is rock mass friction angle, which can be obtained from indoor tests. This equation is only applicable to rock mass with geological strength index is within the range of $25 < \text{GSI} < 75$. When $\text{GSI} \leq 25$, the value of ψ is considered to be 0.

2.3.3. Nonlinear dilatancy angle model of rock mass

Hoek et al. reported rocks show different yield failure under different triaxial confining pressure. By observing the stress-strain relationship curves of rock mass, it was found that the influence of confining pressure on the dilatancy behavior of rock mass was also very strong [24]. Zhao et al. concluded that rock specimens had large volume expansions under low confining pressure conditions by the study of the dilatancy angle curves of sandstone specimens with the change of shear strain, [25]. The optimal fitting equation for dilatancy angle by changing plastic shear strain without considering confining pressure effect was obtained as:

$$\psi = ab\left[\exp\left(-b\gamma_p\right) - \exp\left(-c\gamma_p\right)\right] / (c-b) \tag{2.10}$$

where a, b, and c are all fitting constants.

Based on the study of Zhao et al., combined with the strain-softening model of jointed rock mass, it was considered that the stress required to reach the yield stage of jointed rock mass under different GSI strength grades was different, and the required confining pressure after reaching the peak intensity was also different. In this paper, the confining pressures of surrounding rock after plastic softening failure were simplified to be $\sigma_3 = 0.5(p_i^* p_i^{**})$ and the relationship between sandstone dilatancy angle and plastic shear strain based on the GSI index was proposed. It can be seen from Fig. 6 that with the decrease of GSI indices of surrounding rock, the peak value of nonlinear dilatancy angle of rock masses was decreased and the dilatancy angle model was also very different for different rock materials, especially in dilatancy angle peak values and shear strain.

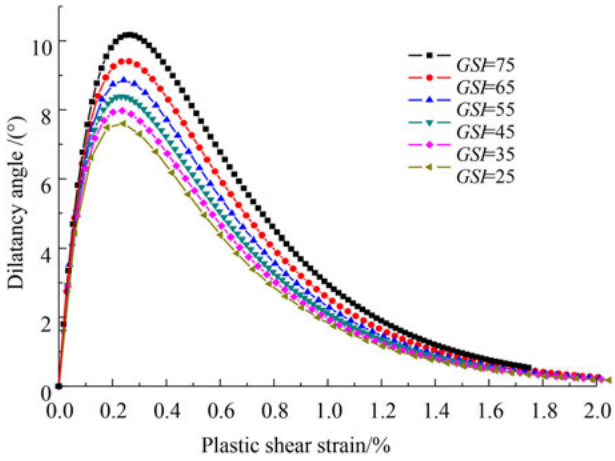

Fig. 6. Improved nonlinear dilatancy angle model of sandstone

3. Numerical analysis of force characteristics of full-length bonded bolts

3.1. Numerical model and parameters

A numerical model for surrounding rock in circular tunnel was developed to analyze the force and support effects of full-length bonded anchors. The boundary conditions of the developed numerical model are shown in Fig. 7a, where the roadway radius was R = 2.5 m, both vertical P_V and the P_H ground stress values were 15MPa, and the side pressure coefficient was 1. Anchors were simulated using cable unit in FLAC^{3D} support structure, which can simulate axial tensile and compression failure characteristics, as well as the shear failure of anchor systems. In order to better simulate stress release during the bolt support process, tunnel load release was simulated under plane strain conditions. The detailed process was as follows: after tunnel excavation, the force acting on the tunnel excavation boundary node was extracted and the same amount of force was applied to the corresponding node of the numerical model. The reduction coefficient is the stress release rate, so as to realize the stress release process of surrounding rock. Bolt units were installed when the stress of the surrounding rock was released by 70% after tunnel excavation. Then, surrounding rock residual stress of the tunnel was released until the system finally reached equilibrium. In the simulation, bolt length was set at 1, 2, 3, 4, 5, and 6 m, bolt diameter was set at 22 mm, and spacing Sr was set at 1.0 m. Bolt arrangement is shown in Fig. 7b.

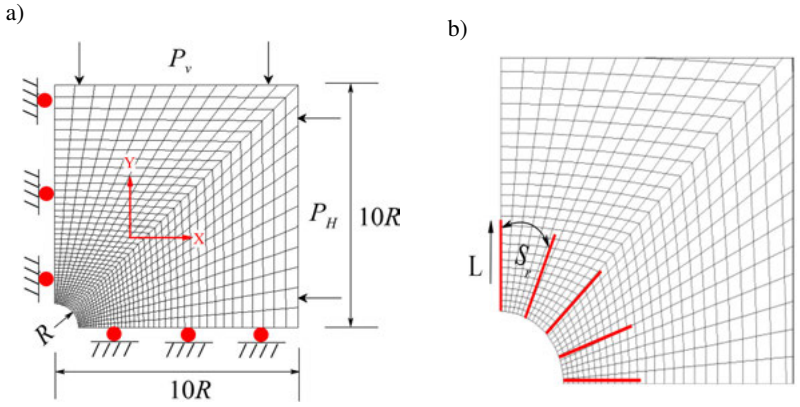

Fig. 7. Numerical calculation model (a) Model size and boundary conditions (b) Anchor layout

In calculations, the lithology of roadway surrounding rock was sandstone with intact rock uniaxial compressive strength σ_{ci} of 65 MPa and Hoek–Brown constant value of m_i = 10. Peak and residual geological strength indices of surrounding rock were calculated to be GSI^p = 60 and GSI^r = 30, respectively. Elastic modulus E was obtained using the following equation [26]:

$$E\,(GPa) = 100\left(\frac{1 - D/2}{1 + e^{[(75+25D-GSI)/11]}}\right) \tag{3.1}$$

where D is the disturbance coefficient. $D = 0.5$ and Poisson's ratio $v = 0.35$. Table function in FLAC^{3D} was used to achieve the variations of softening coefficient η. Table 1 summarizes surrounding rock strength parameters.

Table 1. The values of model parameters

E GPa	v	m^{peak}	m^{res}	s^{peak} 10^{-3}	s^{res} 10^{-3}	c^{peak} MPa	c^{res} MPa	Φ^{peak} °	Φ^{res} °	η^* 10^{-3}
4.7	0.35	2.86	0.97	20.5	0.69	3.78	2.39	36.4	27.5	0.72

3.2. Analysis of calculation results

Fig. 8a shows the relationship between the axial force of anchor bolts with different lengths and the length distribution of bolts obtained by the ideal elastoplastic model. It was observed that anchor length had little effect on the axial forces of anchors and the anchor peak force was about 125 kN. As the length of the bolt increases, the axial force curve of the anchor becomes gentle and drops sharply to zero at a distance of about 20 cm from the end. Fig. 8b shows the curve of the axial force of anchors with anchor length under strain-softening conditions. It was witnessed that the axial force of anchors is highly improved compared to the ideal elastoplastic model and axial force peak at different lengths became closer. The peak point position stayed basically constant and the curve of the curve after the peak is not gentle. This was mainly due to the outward expansion and nonlinear softening of the plastic zone in the strain-softening model, resulting in uneven axial force distribution throughout the anchor.

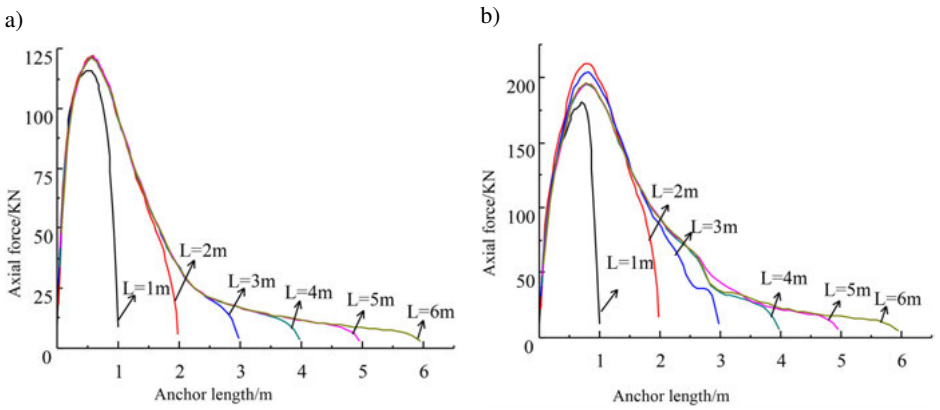

Fig. 8. Axial force at different bolt lengths: a) ideal elastoplastic model, b) strain-softening model

From the shear curves of bolts with different lengths shown in Fig. 9, it was observed that using strain-softening and ideal elastoplastic models, the shear force difference between

the two models was small, and different constitutive models had a slight influence on the shear force of bolts.

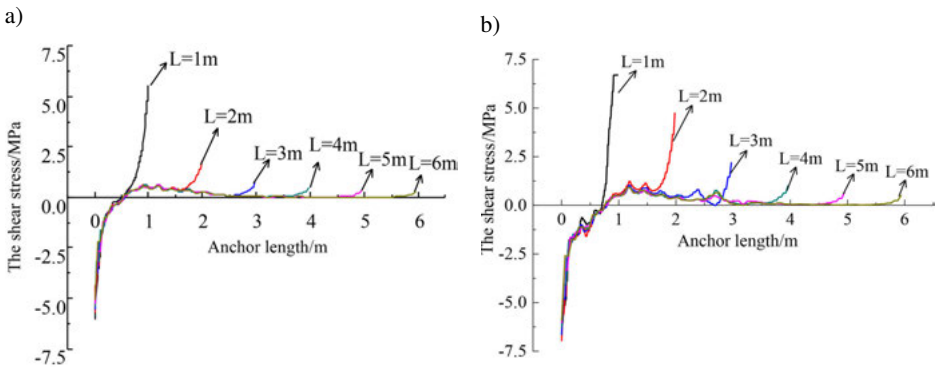

Fig. 9. Shear force of bolts with different lengths: a) Ideal elastoplastic model, b) strain softening model

Fig. 10 shows the axial force of anchors obtained by the application of different pre-stress values for constant bolt length. It was seen from the calculation results that pre-stress had little effect on the peak position and peak size of the anchor shaft force. It was also found that the axial strain of the strain-softening model was the highest while that of the ideal elastoplastic model was the lowest. The results obtained for the two models were quite different. Obviously, using different constitutive models to calculate the stress characteristics of supporting structures gave very different values.

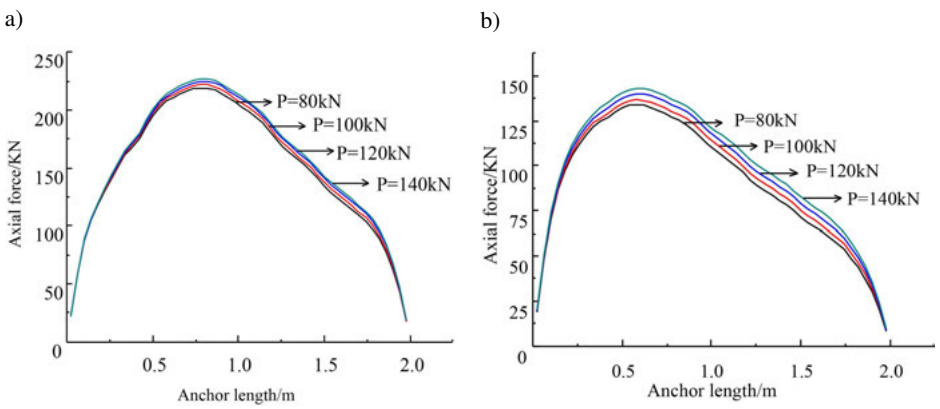

Fig. 10. Axial force of different pre-stressed anchors: a) ideal elastoplastic model, b) strain-softening model

Fig. 11 shows the axial force curves of bolts with different dilatancy angles of surrounding rocks under the three tested model conditions. It could be seen in Fig. 11a that the

increase of dilatancy angle increased the axial force of anchors and the difference in anchor axial forces was changed at different dilatancy angles, such that anchor axial force when $\psi = 15°$ was 1.7 times higher than that when $\psi = 0°$. Fig. 11b shows the distribution curve of anchor axial force obtained using strain-softening and nonlinear dilatancy angle models. By comparing axial force curves of constant and nonlinear dilatancy angles, the curve of anchor axial force in the nonlinear dilatancy angle model was changed between constant dilatancy angles $\psi = 15°$ and $\psi = 0°$. Moreover, the peak position of axial force was closer to the middle of the anchor. It was seen that the dilatancy angle greatly influenced anchor axial force. In support structure design, if the dilatancy angle is neglected, a large error is created in calculation results.

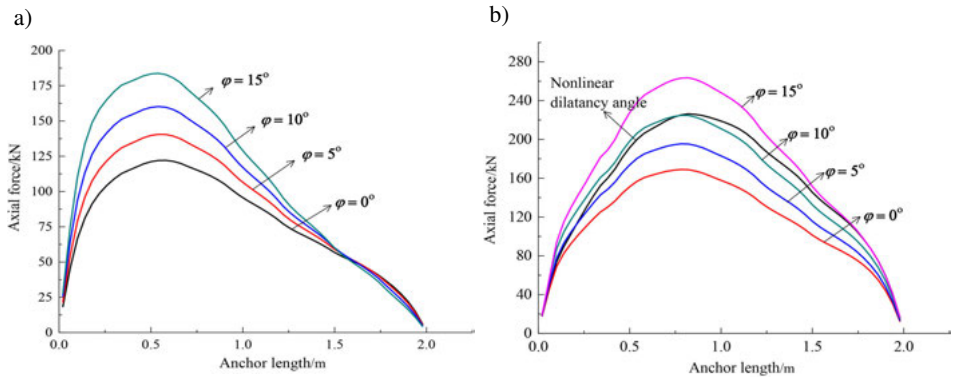

Fig. 11. Axial force of bolts with different dilatancy angles: a) ideal elastoplastic model, b) nonlinear dilatancy angle model

4. Engineering case analysis

4.1. Project overview and numerical model parameters

Mucheng Coal Mine transportation roadway in Inner Mongolia, China is 600 m deep and the design section of roadway is a semi-circular arch type of straight wall. The lithology of the surrounding rock is mainly mudstone and sandstone, mixed with coal line, and the rock mass is relatively soft and broken rock masses (Fig. 12). Hoek–Brown constant $m_i = 8$; Based on uniaxial compressive strength tests on on-site rock samples, $\sigma_{ci} = 35$ MPa. According to the disturbance situation on-site, the disturbance coefficient was calculated to be $D = 0.5$.

The peak geological and residual strength indices of rock masses were estimated to be $\mathrm{GSI}^p = 52$ and $\mathrm{GSI}^r = 30$ from on-site observation of the lithology on excavation surface. Vertical and horizontal ground stress values were $P_V = 17$ MPa and $P_H = 12.5$ MPa, respectively. Anchor net spray support was adopted in the design, where full-length bonded rebar anchors with a spacing of 0.8×0.8 m, length of 2.2 m, and diameter of 22 mm.

Fig. 12. Rock samples obtained on-site and post-fracture characteristics

The numerical calculation model applied in this work is depicted in Fig. 13 and calculation parameters are listed in Table 2.

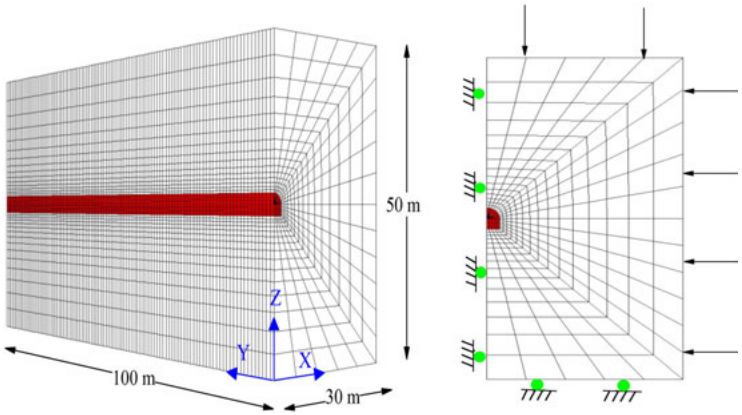

Fig. 13. Numerical calculation model of transport roadway in Mucheng Coal Mine

Table 2. The values of model parameters

E GPa	v	m^{peak}	m^{res}	s^{peak} 10^{-3}	s^{res} 10^{-3}	c^{peak} MPa	c^{res} MPa	Φ^{peak} °	Φ^{res} °	η^* 10^{-3}
2.4	0.25	2.0	0.85	6.7	0.47	3.15	2.26	33.4	26.6	2.0

4.2. Analysis of calculation results

In this paper, by constructing a 3D numerical model, the numerical calculation of full-length bonded anchor supports was carried out and numerical results were compared with experimental findings. It can be seen from Fig. 14 that surrounding rock displacement

in the dome was increased by increasing the distance from the excavation surface and the experimental results revealed that the deformation of surrounding rocks tended to be stable when it was about 40 m away from working surface. Numerical results revealed that the deformation curves of surrounding rocks obtained according to the ideal elastoplastic model were quite different from experimental values and surrounding rock tended to be stabilized 25 m away from working surface. Numerical results obtained by strain-softening model based on nonlinear dilatancy angle were close to experimental values. Under the action of full-length bonded anchor support, surrounding rock tended to be stable 45 m away from working surface. Obviously, numerical results obtained from the strain-softening model based on nonlinear dilatancy angle were closer to actual engineering conditions.

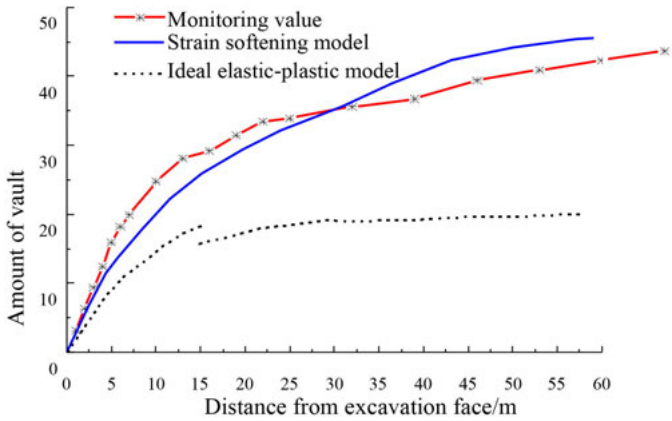

Fig. 14. Tunnel vault subsidence curve

5. Conclusions

1. Based on the quantitative GSI system, considering the volume deformations of rock masses, a nonlinear dilatancy angle model was proposed. The model reflected the variation of dilatancy angles of rock masses with plastic shear strain. With the decrease of GSI indices of surrounding rocks, peak values of nonlinear dilatancy angles of rock masses were decreased.
2. Anchor axial forces calculated by the elastoplastic model were lower than numerical results obtained while considering strain-softening and different constitutive models had little effect on anchor shear force. When a preload was applied to full-length bonded anchors, anchor axial forces were only slightly changed.
3. Constant dilatancy angle greatly affected anchor axial force. The nonlinear dilatancy angle proposed in this paper was closer to the actual situation of the project by experimental measurements and numerical analyses. The calculation results can provide support for the design of deep roadway engineering.

References

[1] Q.H. Qian, "The new development of nonlinear rock mechanics – many key problem of deep rock mass mechanics", in *The Eighth National Rock Mechanics and Engineering Academic Memoir*, Beijing: Science Press, 2004 (in Chinese).

[2] C. González-Nicieza, A.E. Álvarez-Vigil, A. Menéndez-Díaz, C. González-Palacio. Influence of the depth and shape of a tunnel in the application of the convergence–confinement method. *Tunnelling and Underground Space Technology*, 2008, vol. 23, no. 1, pp. 25–37, DOI: 10.1016/j.tust.2006.12.001.

[3] H. Kang, J. Wang, J. Lin, "Case studies of rock bolting in coal mine roadways", *Chinese Journal of Rock Mechanics Engineering*, 2010, vol. 29, no. 4, pp. 649–665 (in Chinese).

[4] Z.M. Shi, L.Liu, M. Peng, C.C. Liu, F.J. Tao, C.S. Liu, "Non-destructive testing of full-length bonded rock bolts based on HHT signal analysis", *Journal of Applied Geophysics*, 2018, vol. 151, pp. 47–65, DOI: 10.1016/j.jappgeo.2018.02.001.

[5] X. Feng, N. Zhang, F. He, et al., "Implementation of a Pretensioned, Fully Bonded Bolting System and Its Failure Mechanism Based on Acoustic Emission: A Laboratorial and Field Study", *Geotechnical Testing Journal*, 2017, vol. 40, no. 6, DOI: 10.1520/GTJ20160157.

[6] S. Yang, W.Xu, Q. Huang, "Analysis on the Bolt Deformation as Result of Joint Shear Displacement", *Chinese Journal of Rock Mechanics and Engineering*, 2004 (in Chinese).

[7] Q.H. Wu, F.J. Zhao, S.M. Wang, Z.H. Zhou, B. Wang, Y. Li, "Mechanical response characteristics of full grouted rock bolts subjected to dynamic loading", *Rock and Soil Mechanics*, 2019, vol. 40, no. 3, pp. 942–950+1004 (in Chinese).

[8] B. Liu, L. Huang, D.Y. Li, "Analytical Formulation on the Mechanical Behavior of Anchorage Interface for Full-Length Bonded Bolt", *Applied Mechanics and Materials*, 2012, vol. 166–169, pp. 3254–3257, DOI: 10.4028/www.scientific.net/AMM.166-169.3254.

[9] P.P. Oreste, "Analysis of structural interaction in tunnels using the convergence–confinement approach", *Tunnelling and Underground Space Technology Incorporating Trenchless Technology Research*, 2003, vol. 18, no. 4, pp. 347–363, DOI: 10.1016/S0886-7798(03)00004-X.

[10] X. Yao, N. Li, Y. Chen, "Stress analysis of full-length adhesive bolt in tunnel", *J. Rock Mech. Eng*., 2005, vol. 13, pp. 2272–2276 (In Chinese).

[11] X.G. Zhao, M. Cai, P. Jia, "Mutual influence between shear dilatation of rock mass and rebar support around underground excavation", *Chinese Journal of Rock Mechanics and Engineering*, 2010, vol. 29, no. 10, pp. 2056–2063 (In Chinese).

[12] F. Salehnia, F. Collin, R. Charlier, "On the Variable Dilatancy Angle in Rocks Around Underground Galleries", *Rock Mechanics and Rock Engineering*, 2016, vol. 50, pp. 587–601, DOI: 10.1007/s00603-016-1126-6.

[13] L. Cheng, J. Xu, T. Lu, "Effects of Tectonic Stress on Stability of Dilatancy Characteristic Soft Rock Roadway Intersection in Deep Underground", *Disaster Advances*, 2012, vol. 5, no. 4, pp. 1190–1195.

[14] Q.S. Zhao, C.H. Zhang, "Dilatancy Model of Heterogeneous Rock with Confining Stress", *Civil Engineering in China – Current Practice and Research Report: Proceedings of the 2nd International Conference on Civil Engineering*, pp. 297–303 (in Chinese).

[15] B. Wang, J.B. Zhu, A.Q. Wu, et al., "Experimental study of nonlinear dilatancy characteristics based on the damage-controlled method", *Rock and Soil Mechanics*, 2015, vol. 36, no. 4, pp. 981–987, DOI: 10.16285/j.rsm.2015.04.010.

[16] L.R. Alejano, E. Alonso, "Considerations of the dilatancy angle in rocks and rock masses", *International Journal of Rock Mechanics and Mining Scienc*es, 2005, vol. 42, no. 4, pp. 481–507, DOI: 10.1016/j.ijrmms.2005.01.003.

[17] L.R. Alejano, E. Alonso, F. Varas, "A Model to Estimate the Dilatancy Angle of Rock Masses", in *Impact of Human Activity on the Geological Environment- International Symposium of the International Society for Rock Mechanics*, 2005. [Online]. Available: https://onepetro.org/ISRMEUROCK/proceedings-abstract/EUROCK05/All-EUROCK05/ISRM-EUROCK-2005-003/38189.

[18] E. Hoek, E.T. Brown, "Practical estimates of rock mass strength" *International Journal of Rock Mechanics and Mining Sciences*, 1997, vol. 34, no. 8, pp. 1165–1186, DOI: 10.1016/S1365-1609(97)80069-X.

[19] M. Cai, P.K. Kaiser, H. Uno, et al., "Estimation of rock mass deformation modulus and strength of jointed hard rock masses using the GSI system", *International Journal of Rock Mechanics and Mining Sciences*, 2004, vol. 41, no. 1, pp. 3–19, DOI: 10.1016/S1365-1609(03)00025-X.

[20] E. Hoek, C.T. Caranza-Torres, B. Corcum, "Hoek–Brown failure criterion", in *Proceedings of the North American Rock Mechanics Society. Toronto: Mining Innovation and Technology*, 2002, pp. 267–273.

[21] M. Cai, P.K. Kaiser, Y. Tasaka, et al., "Determination of residual strength parameters of jointed rock masses using the GSI system", *International Journal of Rock Mechanics and Mining Sciences*, 2007, vol. 44, no. 2, pp. 247–265, DOI: 10.1016/j.ijrmms.2006.07.005.

[22] L.R. Alejano, A. Rodríguez-Dono, M. Veiga, "Plastic radii and longitudinal deformation profiles of tunnels excavated in strain-softening rock masses", *Tunnelling and Underground Space Technology incorporating Trenchless Technology Research*, 2012, vol. 30, pp. 169–182, DOI: 10.1016/j.tust.2012.02.017.

[23] L.R. Alejano, E. Alonso, "Considerations of the dilatancy angle in rocks and rock masses", *International Journal of Rock Mechanics and Mining Sciences*, 2005, vol. 42, no. 4, pp. 481–507, DOI: 10.1016/j.ijrmms.2005.01.003.

[24] E. Hoek, M.S. Diederichs, "Empirical estimation of rock mass modulus", *International Journal of Rock Mechanics and Mining Sciences*, 2006, vol. 43, no. 2, pp. 203–215, DOI: 10.1016/j.ijrmms.2005.06.005.

[25] X.G. Zhao, M. Cai, "A mobilized dilation angle model for rocks", *International Journal of Rock Mechanics and Mining Sciences*, 2010, vol. 47, no. 3, pp. 368–384, DOI: 10.1016/j.ijrmms.2009.12.007.

[26] L.R. Alejano, E. Alonso, A. Rodríguez-Dono, et al., "Application of the convergence-confinement method to tunnels in rock masses exhibiting Hoek–Brown strain-softening behaviour", *International Journal of Rock Mechanics and Mining Sciences*, 2010, vol. 47, no. 1, pp. 150–160, DOI: 10.1016/j.ijrmms.2009.07.008.

Received: 30.11.2021, Revised: 7.12.2021